Hindawi Publishing Corporation
Mathematical Problems in Engineering
Volume 2012, Article ID 287195, 31 pages
doi:10.1155/2012/287195

*Research Article*

# Vehicle Sliding Mode Control with Adaptive Upper Bounds: Static versus Dynamic Allocation to Saturated Tire Forces

**Ali Tavasoli and Mahyar Naraghi**

*Department of Mechanical Engineering, Amirkabir University of Technology, 424 Hafez Avenue, Tehran 15914, Iran*

Correspondence should be addressed to Mahyar Naraghi, naraghi@aut.ac.ir

Received 20 December 2011; Accepted 13 February 2012

Academic Editor: Alexander P. Seyranian



Nonlinear vehicle control allocation is achieved through distributing the task of vehicle control among individual tire forces, which are constrained to nonlinear saturation conditions. A high-level sliding mode control with adaptive upper bounds is considered to assess the body yaw moment and lateral force for the vehicle motion. The proposed controller only requires the online adaptation of control gains without acquiring the knowledge of upper bounds on system uncertainties. Static and dynamic control allocation approaches have been formulated to distribute high-level control objectives among the system inputs. For static control allocation, the interior-point method is applied to solve the formulated nonlinear optimization problem. Based on the dynamic control allocation method, a dynamic update law is derived to allocate vehicle control to tire forces. The allocated tire forces are fed into a low-level control module, where the applied torque and active steering angle at each wheel are determined through a slip-ratio controller and an inverse tire model. Computer simulations are used to prove the significant effects of the proposed control allocation methods on improving the stability and handling performance. The advantages and limitations of each method have been discussed, and conclusions have been derived.

## 1. Introduction

In recent years by rapid emergence of electronic control devices, employing all available actuators, or individual tire forces, for ground vehicle control has become possible [1]. The vehicle motion is governed by tire forces which are constrained based on friction circle notion. Thus, tire saturation constraints must be taken into account for a proper control design. The problem of optimal actuators selection to execute a control task, while minimizing effort and satisfying constraints, is known as Control Allocation (CA). To tackle actuator constraints in control design of a general over-actuated nonlinear system, two approaches of Static

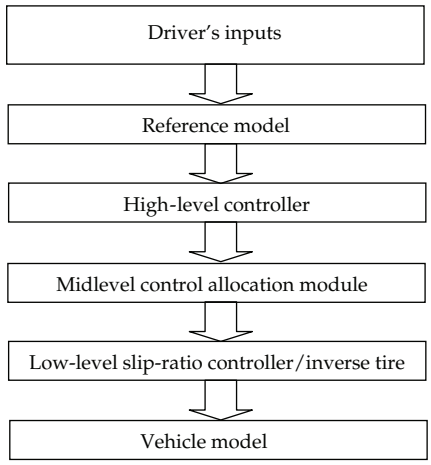


**Figure 1:** Overall structure of the integrated vehicle dynamics control scheme.

Control Allocation (SCA) and Dynamic Control Allocation (DCA) are proposed. In SCA, the total body forces/moments of a high-level controller are allocated to available actuators by optimizing a suitable cost function at each sampling time, whereas DCA generates a dynamic update law for actuators. No optimization problem needs to be solved by DCA.

In the field of Integrated Vehicle Dynamics Control (IVDC), Optimal Distribution of tire Forces (ODF) was introduced to meet various objectives, such as maximizing longitudinal acceleration [2], minimizing total tire workload usage [3], or adaptive-optimal coordination of braking and steering [4]. Attempts to account for actuator constraints were rare in these works.

To allocate control objectives to the actuators with limited amplitude/rate, SCA methods have been subject of different studies. Algorithms using various optimization methods, such as quadratic programming [5], multiparametric nonlinear programming [6], and fixed point [1], were developed. Kou [7] proposed an SCA scheme based on the model predictive control and fixed point method. The main problem in static control allocation is its computational burden for practical applications, due to numerical solution of a constrained optimization problem at each sampling instant.

To deal with this difficulty, Johansen [8] developed a dynamic control allocation method for a particular class of nonlinear systems. In this regard, a dynamic update law leads the desired actuator efforts to converge to the solution of a definite optimization problem, without solving the optimization problem. DCA was extended for systems with unknown parameters [9] and applied to vehicle yaw control [10].

This paper addresses nonlinear vehicle CA constrained to tire saturation conditions. Referring to schematic view of IVDC structure in Figure 1, the required body lateral force and yaw moment for vehicle motion are determined by a high-level sliding mode enhanced adaptive controller. The adaptive control methodology is utilized to update the perturbation and sliding mode control gains, so that the upper bounds of uncertainties are not required to be known in advance. Then, the body force and moment, along with the driver's desired braking force, are allocated to individual lateral and longitudinal forces of each tire. Considering tires saturation induces nonlinear constraints in CA problem. To tackle this problem, we look into SCA and DCA methods for vehicle control. For static allocation purpose, the interior point is formulated and employed to solve the nonlinear inequality

constrained optimization problem. To formulate dynamic allocation control for the proposed problem, a dynamic update law is derived and utilized in the IVDC scheme. The desired lateral force of each tire by CA modules is mapped into the corresponding active steering angle through an inverse tire model. In addition, the desired longitudinal forces are tracked by a low-level slip-ratio control scheme. Simulation results are conducted to evaluate the effectiveness of each method.

The rest of the paper is organized as follows. The high-level control is described next. Section 3 presents the formulation of optimal distribution of tire forces in IVDC considering nonlinear tire saturation constraints. In Section 4, the SCA is formulated based on the interior-point method. In Section 5, the DCA approach is utilized to derive an optimized dynamic update law for individual tire forces. The low-level slip-ratio controller has been addressed in Section 6. Sections 7 and 8 are devoted to simulation results and concluding remarks.

## 2. High-Level Sliding Mode Control with Adaptive Upper Bounds

In this section we first design a high-level controller for vehicle handling and stability based on the conventional Sliding Mode Control (SMC), then an SMC with updated upper bounds of uncertainties is considered.

### 2.1. Conventional Sliding Mode Control

In general, vehicle handling and stability are achieved through the control of yaw rate and side-slip angle, respectively. The design procedure is based on the 2DoF vehicle model, where the basic equations are [11]

$$\begin{aligned} mV\left(\dot{\beta}+r\right) &= Y, \\ I_z\dot{r} &= M, \end{aligned} \tag{2.1}$$

where $m$ and $I_z$ denote the total mass and yaw moment of inertia, from which only the estimates of $\widehat{m}$ and $\widehat{I}_z$ are available, and $V$ is the vehicle velocity. $\beta$ and $r$ stand for the actual vehicle side-slip angle and the yaw rate, respectively. $M$ and $Y$ are sum of external moments in the yaw direction and lateral forces acting on the vehicle, respectively. To account for the unmodelled dynamics and uncertainties in modelling the actual nonlinear vehicle dynamics, the unknown, but bounded, disturbance terms, $\omega_\beta$ and $\omega_r$, are embedded into each channel to get

$$mV\left(\dot{\beta}+r\right) = Y+\omega_\beta, \tag{2.2}$$

$$I_z\dot{r} = M+\omega_r. \tag{2.3}$$

To design the total lateral force ($Y$), for a zero desired side-slip angle, the sliding surface, $s_\beta$, is selected as

$$s_\beta = \beta. \tag{2.4}$$

Differentiating this equation and considering (2.2),

$$\dot{s}_\beta = \frac{Y}{mV} - r + \frac{\Delta_\beta}{m}, \tag{2.5}$$

where the term $\Delta_\beta = \omega_\beta / V$ is assumed to be bounded by a known value $\overline{\Delta}_\beta$:

$$\left|\Delta_\beta\right| < \overline{\Delta}_\beta. \tag{2.6}$$

To guarantee the sliding condition [12]

$$s_\beta \dot{s}_\beta < 0, \tag{2.7}$$

the desired body lateral force is considered as

$$Y = V\left(\hat{m}r + v_\beta\right) \tag{2.8}$$

in which $\hat{m}$ is our estimate of $m$ and $v_\beta$ is to be designed. Insert (2.8) into (2.5) to get the left side of (2.7) as

$$s_\beta \dot{s}_\beta = s_\beta m^{-1}\left(\Delta_\beta + v_\beta + \tilde{m}r\right), \tag{2.9}$$

where the mass estimation error $\tilde{m} = \hat{m} - m$ is assumed to satisfy

$$|\tilde{m}| = |\hat{m} - m| < \overline{m}, \quad \overline{m} > 0, \tag{2.10}$$

whose combination with (2.9) and (2.6) results in

$$s_\beta \dot{s}_\beta \le m^{-1}\left(s_\beta v_\beta + \left|\Delta_\beta\right|\left|s_\beta\right| + |\tilde{m}||r|\left|s_\beta\right|\right) < m^{-1}\left(s_\beta v_\beta + \overline{\Delta}_\beta\left|s_\beta\right| + \overline{m}|r|\left|s_\beta\right|\right). \tag{2.11}$$

To achieve (2.7), $v_\beta$ is considered to be

$$v_\beta = -k_\beta \operatorname{sgn}\left(s_\beta\right), \tag{2.12}$$

where $\operatorname{sgn}(\cdot)$ is the signum function, and

$$k_\beta > \overline{\Delta}_\beta + \overline{m}|r| + \eta_\beta, \quad \eta_\beta > 0. \tag{2.13}$$

By substituting (2.12) into (2.8), the desired body lateral force is attained. To mitigate the problem of chattering, the sign function is replaced by saturation function with a boundary layer thickness of $\Phi_\beta > 0$. Thus, the final control law becomes

$$Y = V\left(\hat{m}r - k_\beta \operatorname{sat}\left(\frac{s_\beta}{\Phi_\beta}\right)\right). \tag{2.14}$$

In order to design the body yaw moment ($M$), for tracking the desired yaw rate ($r_d$), the sliding surface, $s_r$, is adopted as

$$s_r = (r - r_d) + \lambda_r \int_0^t (r - r_d) d\tau, \quad \lambda_r > 0, \tag{2.15}$$

where the integral term is used to mitigate the undesirable yaw angle offset and to ensure the desired vehicle heading. Differentiating (2.15) along with (2.3) leads to

$$\dot{s}_r = \frac{M}{I_z} + \frac{\omega_r}{I_z} - \tau, \qquad \tau = \dot{r}_d - \lambda_r (r - r_d). \tag{2.16}$$

The design process of the desired body yaw moment is similar to that of (2.14):

$$M = \widehat{I}_z (\dot{r}_d - \lambda_r (r - r_d)) - k_r \operatorname{sat}\left(\frac{s_r}{\Phi_r}\right), \quad \Phi_r > 0, \tag{2.17}$$

where $\widehat{I}_z$ is an estimate of $I_z$ and

$$k_r > \overline{\Delta}_r + \overline{I}_z |\dot{r}_d - \lambda_r (r - r_d)| + \eta_r, \quad \eta_r > 0, \tag{2.18}$$

with $\overline{\Delta}_r > 0$ and $\overline{I}_z > 0$ being the upper bounds for $|\omega_r|$ and $|\widetilde{I}_z| = |\widehat{I}_z - I_z|$, respectively.

### 2.2. Sliding Mode Control with Adaptive Upper Bounds

From (2.13) and (2.18) it can be observed that the selection of the SMC gains $k_\beta$ and $k_r$ depends on upper bounds of uncertainties in vehicle dynamics and body mass and inertia, that is, $\overline{\Delta}_r$, $\overline{\Delta}_\beta$, $\overline{m}$, and $\overline{I}_z$. In practice, uncertainties and disturbances depend primarily on the highly nonlinear dynamics of vehicle and tire which are not completely known, and one cannot determine their exact bounds too. Therefore, no universal method is available yet to tune the controller gains and these gains should be tuned by trial and error approach in practical implementations. In this regard, the controller tends to be overconservative, which may induce poor tracking performance as well as undesirable oscillations in control signal. To overcome this drawback, adaptive control methodology with control parameters updated online is a promising approach. In this section, we use the adaptive control technique to attain a sliding mode controller with adaptive upper bounds. To design sliding mode controls with variable gains, the following modified control laws are established:

$$Y = V\left(\widehat{m} r - \left(\widehat{k}_{\beta 1} + \widehat{k}_{\beta 2} |r|\right) \operatorname{sgn}(s_\beta)\right), \tag{2.19}$$

$$M = \widehat{I}_z \tau - \left(\widehat{k}_{r1} + \widehat{k}_{r2} |\tau|\right) \operatorname{sgn}(s_r), \tag{2.20}$$

where

$$\tau = \dot{r}_d - \lambda_r (r - r_d) \tag{2.21}$$

and the varying controller gains are updated as follows:

$$\dot{\hat{k}}_{\beta 1} = \gamma_{\beta 1}^{-1}\left|s_\beta\right|, \quad \gamma_{\beta 1} > 0, \tag{2.22}$$

$$\dot{\hat{k}}_{\beta 2} = \gamma_{\beta 2}^{-1}|r|\left|s_\beta\right|, \quad \gamma_{\beta 2} > 0, \tag{2.23}$$

$$\dot{\hat{k}}_{r1} = \gamma_{r1}^{-1}|s_r|, \quad \gamma_{r1} > 0, \tag{2.24}$$

$$\dot{\hat{k}}_{r2} = \gamma_{r2}^{-1}|\tau||s_r|, \quad \gamma_{r2} > 0. \tag{2.25}$$

Assume that there are positive constants $k_{\beta 1}^d$, $k_{\beta 2}^d$, $k_{r1}^d$, and $k_{r2}^d$ that satisfy

$$k_{\beta 1}^d > \left|\Delta_\beta\right|, \qquad k_{\beta 2}^d > |\tilde{m}|, \tag{2.26}$$

$$k_{r1}^d > |\Delta_r|, \qquad k_{r2}^d > \left|\tilde{I}_z\right|. \tag{2.27}$$

It should be noted that we need only to assure that such constants exist without acquiring the knowledge of these upper bounds to use in control laws. Also, consider

$$\tilde{k}_{\beta 1} = \hat{k}_{\beta 1} - k_{\beta 1}^d, \qquad \tilde{k}_{\beta 2} = \hat{k}_{\beta 2} - k_{\beta 2}^d, \tag{2.28}$$

$$\tilde{k}_{r1} = \hat{k}_{r1} - k_{r1}^d, \qquad \tilde{k}_{r2} = \hat{k}_{r2} - k_{r2}^d. \tag{2.29}$$

Then, the stability of the considered adaptive-sliding mode control laws can be shown through Lyapunov candidates:

$$V_\beta = \frac{m}{2}s_\beta^2 + \frac{1}{2}\gamma_{\beta 1}\tilde{k}_{\beta 1}^2 + \frac{1}{2}\gamma_{\beta 2}\tilde{k}_{\beta 2}^2, \tag{2.30}$$

$$V_r = \frac{I_z}{2}s_r^2 + \frac{1}{2}\gamma_{r1}\tilde{k}_{r1}^2 + \frac{1}{2}\gamma_{r2}\tilde{k}_{r2}^2. \tag{2.31}$$

To prove the stability of side-slip angle under (2.19) with adaptation laws (2.22) and (2.23), first insert (2.19) into (2.5) so that

$$m\dot{s}_\beta = \left(\tilde{m}r + \Delta_\beta - \left(\hat{k}_{\beta 1} + \hat{k}_{\beta 2}|r|\right)\operatorname{sgn}\left(s_\beta\right)\right). \tag{2.32}$$

Then, differentiate (2.30) to get

$$\dot{V}_\beta = ms_\beta\dot{s}_\beta + \left(\gamma_{\beta 1}\tilde{k}_{\beta 1}\dot{\tilde{k}}_{\beta 1} + \gamma_{\beta 2}\tilde{k}_{\beta 2}\dot{\tilde{k}}_{\beta 2}\right). \tag{2.33}$$

Replacing (2.32) in (2.33) and considering (2.28), we have that

$$\begin{aligned}\dot{V}_\beta = &\left(\tilde{m}r + \Delta_\beta - \left(\hat{k}_{\beta1} + \hat{k}_{\beta2}|r|\right)\operatorname{sgn}(s_\beta)\right)s_\beta + \left(\gamma_{\beta1}\dot{\hat{k}}_{\beta1}\hat{k}_{\beta1} + \gamma_{\beta2}\dot{\hat{k}}_{\beta2}\hat{k}_{\beta2}\right)\\ &- \left(\gamma_{\beta1}\dot{\hat{k}}_{\beta1}k^d_{\beta1} + \gamma_{\beta2}\dot{\hat{k}}_{\beta2}k^d_{\beta2}\right).\end{aligned} \tag{2.34}$$

Using adaptation laws (2.22) and (2.23) in (2.34) and considering (2.26) results in

$$\begin{aligned}\dot{V}_\beta &= (\tilde{m}r + \Delta_\beta)s_\beta - k^d_{\beta1}|s_\beta| - k^d_{\beta2}|r||s_\beta| \le (|\tilde{m}||r| + |\Delta_\beta|)|s_\beta| - k^d_{\beta1}|s_\beta| - k^d_{\beta2}|r||s_\beta|\\ &= \left(|\tilde{m}| - k^d_{\beta2}\right)|r||s_\beta| + \left(|\Delta_\beta| - k^d_{\beta1}\right)|s_\beta| < 0,\end{aligned} \tag{2.35}$$

where we use $s_\beta \operatorname{sgn}(s_\beta) = |s_\beta|$. Accordingly, the convergence of $s_\beta$ to zero and also boundedness of $\tilde{k}_{\beta1}$ and $\tilde{k}_{\beta2}$ are resulted by Barbalat's lemma [12].
In an identical way, the stability of the yaw motion can be demonstrated, first, by combining (2.16) and (2.20) so that

$$I_z\dot{s}_r = \tilde{I}_z\tau + \Delta_r - \left(\hat{k}_{r1} + \hat{k}_{r2}|\tau|\right)\operatorname{sgn}(s_r). \tag{2.36}$$

Differentiate (2.31) and replace (2.36) for $I_z\dot{s}_r$ to get

$$\dot{V}_r = \left(\tilde{I}_z\tau + \Delta_r - \left(\hat{k}_{r1} + \hat{k}_{r2}|\tau|\right)\operatorname{sgn}(s_r)\right)s_r + \left(\gamma_{r1}\dot{\hat{k}}_{r1}\hat{k}_{r1} + \gamma_{r2}\dot{\hat{k}}_{r2}\hat{k}_{r2}\right) - \left(\gamma_{r1}\dot{\hat{k}}_{r1}k^d_{r1} + \gamma_{r2}\dot{\hat{k}}_{r2}k^d_{r2}\right). \tag{2.37}$$

Using adaptation laws (2.24) and (2.25) as well as the inequalities in (2.27), we have that

$$\begin{aligned}\dot{V}_r &= \left(\tilde{I}_z\tau + \Delta_r\right)s_r - k^d_{r1}|s_r| - k^d_{\beta2}|\tau||s_r| \le \left(\left|\tilde{I}_z\right||\tau| + |\Delta_r|\right)|s_r| - k^d_{r1}|s_r| - k^d_{r2}|\tau||s_r|\\ &= \left(\left|\tilde{I}_z\right| - k^d_{r2}\right)|\tau||s_r| + \left(|\Delta_r| - k^d_{r1}\right)|s_r| < 0.\end{aligned} \tag{2.38}$$

Thus, according to the Barbalat's Lemma, the system state can be driven to the sliding surface $s_r$ and the controller gains $\tilde{k}_{r1}$ and $\tilde{k}_{r2}$ will be bounded. Furthermore, to tackle the chattering problem saturation function is used to derive the final adaptive control laws

$$\begin{aligned}\Upsilon &= V\left(\hat{m}r - \left(\hat{k}_{\beta1} + \hat{k}_{\beta2}|r|\right)\operatorname{sat}\left(\frac{s_\beta}{\Phi_\beta}\right)\right),\\ M &= \hat{I}_z\tau - \left(\hat{k}_{r1} + \hat{k}_{r2}|\tau|\right)\operatorname{sat}\left(\frac{s_r}{\Phi_r}\right).\end{aligned} \tag{2.39}$$

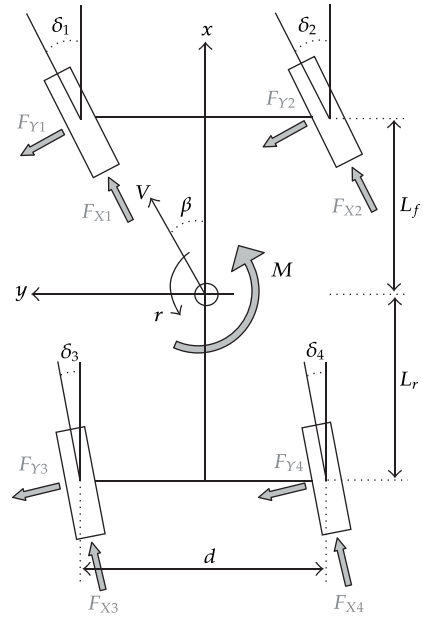


**Figure 2:** Schematic view of forces acting on the vehicle.

## 3. Control Allocation in Vehicle System

The total body lateral force and yaw moment, as well as the braking acceleration command by driver, are generated by longitudinal and lateral forces of each tire. In this paper, a 4-wheel vehicle system with each wheel being braked/derived and steered independently is considered. Such a full tire-actuated vehicle can be available through X-by-wire systems [1, 13]. Thus, the overall control system contains eight actuators and only three control objectives, raising an overactuated control system. A general approach to resolve redundancy is to optimize a cost function for specific performance. The well-accepted cost function in IVDC is the sum of work load of four wheels:

$$f = \sum_{i=1}^{4} A_i \frac{X_i^2 + Y_i^2}{\left(\mu_i Z_i\right)^2}, \tag{3.1}$$

where $i$ denotes wheel number, $X_i$ and $Y_i$ stand for desired values of longitudinal force, $F_{xi}$, and lateral force, $F_{yi}$, $Z_i$ is the vertical load, all defined in the vehicle body fixed coordinate system, as shown in Figure 2, $A_i$ is the weighting coefficient and $\mu_i$ is the friction coefficient, of the $i$th tire. Defining the $8 \times 1$ actuator vector of $\mathbf{u}$ as

$$\mathbf{u} = [X_1 \;\; X_2 \;\; X_3 \;\; X_4 \;\; Y_1 \;\; Y_2 \;\; Y_3 \;\; Y_4]^T, \tag{3.2}$$

the cost function is written in matrix form

$$f(\mathbf{u}) = \mathbf{u}^{\mathbf{T}}\mathbf{W}\mathbf{u} \tag{3.3}$$

in which $\mathbf{W_{8\times 8}}$ is a diagonal weighting matrix. To get $Y$ and $M$, by assuming small steering angles in Figure 2, individual tire forces must satisfy the equality constraints:

$$Y = \sum_{i=1}^{4} Y_i, \tag{3.4}$$

$$M = \sum_{i=1}^{2} \left(L_f Y_i - L_r Y_{(i+2)}\right) + \frac{d}{2} \sum_{i=1}^{2} \left(X_{(2i)} - X_{(2i-1)}\right). \tag{3.5}$$

Also, the longitudinal acceleration, $a_x$, by driver is generated by longitudinal forces

$$X = ma_x = \sum_{i=1}^{4} X_i. \tag{3.6}$$

Equations (3.4)–(3.6) can be expressed in linear matrix form as

$$\mathbf{Au} = \mathbf{v}, \tag{3.7}$$

where $\mathbf{A} \in \Re^{3\times 8}$ is a constant matrix and the vector of generalized forces/moment, $\mathbf{v}$, is given by

$$\mathbf{v} = [X \;\; Y \;\; M]^T. \tag{3.8}$$

On the other hand, the resultant force of each tire is constrained to friction circle

$$\left(\mu_i Z_i\right)^2 - \left(X_i^2 + Y_i^2\right) \geq 0 \quad (i = 1, \ldots, 4). \tag{3.9}$$

Using (3.2), (3.9) can be written as

$$\left(\mu_i Z_i\right)^2 - \left(u_i^2 + u_{i+4}^2\right) \geq 0 \quad (i = 1, \ldots, 4). \tag{3.10}$$

or

$$\mathbf{C_I}(\mathbf{u}) \geq \mathbf{0}, \tag{3.11}$$

where $\mathbf{C_I}$ is a $4 \times 1$ vector with the $i$th component

$$C_{Ii}(u_i) = \left(\mu_i Z_i\right)^2 - \left(u_i^2 + u_{i+4}^2\right) \quad (i = 1, \ldots, 4). \tag{3.12}$$

The optimization problem is summarized as follows:

$$\begin{aligned} &\text{minimize } f(\mathbf{u}) = \mathbf{u}^{\mathbf{T}}\mathbf{W}\mathbf{u}, \\ &\text{subject to } \begin{cases} \text{linear equality constraints,} & \mathbf{A}\mathbf{u} = \mathbf{v}, \\ \text{nonlinear inequality constraints,} & \mathbf{C_I}(\mathbf{u}) \geq \mathbf{0}. \end{cases} \end{aligned} \tag{3.13}$$

## 4. Static Control Allocation: Application of Interior-Point Method

SCA solves the optimization problem (3.13) at each sampling instant. A powerful approach for nonlinear programming is the set of interior-point (IP) methods. A benefit of such methods is that the distance from the optimum is always known, so that one can terminate the optimization algorithm when the solution reaches within desired tolerance. Convergence is also uniform toward the optimal solution. The description of IP algorithm in this paper is an excerpt from [14, 15].

### *4.1. Karush-Kuhn-Tucker Conditions*

At the outset to avoid infeasible solutions, the equality constraints are embedded in cost function to get

$$J = \rho\mathbf{u}^{\mathbf{T}}\mathbf{W}\mathbf{u} + (\mathbf{A}\mathbf{u} - \mathbf{v})^{\mathbf{T}}(\mathbf{A}\mathbf{u} - \mathbf{v}), \quad \rho > 0, \tag{4.1}$$

which is written in the quadratic form

$$J = \frac{1}{2}\mathbf{u}^{\mathbf{T}}\mathbf{G}\mathbf{u} + \mathbf{c}^{\mathbf{T}}\mathbf{u} + \mathbf{h}, \tag{4.2}$$

where

$$\mathbf{G} = 2\left(\rho\mathbf{W} + \mathbf{A}^{\mathbf{T}}\mathbf{A}\right), \qquad \mathbf{c} = -2\mathbf{A}^{\mathbf{T}}\mathbf{v}, \qquad \mathbf{h} = \mathbf{v}^{\mathbf{T}}\mathbf{v}. \tag{4.3}$$

IP methods use barrier logarithmic functions to satisfy the inequality constraints. In this regard, the optimization problem turns into

$$\begin{aligned} &\text{minimize} L = \frac{1}{2}\mathbf{u}^{\mathbf{T}}\mathbf{G}\mathbf{u} + \mathbf{c}^{\mathbf{T}}\mathbf{u} + \mathbf{h} - \eta\sum_{i=1}^{4}\log(C_{Ii}), \quad \eta > 0, \\ &\text{subject to} \begin{cases} \mathbf{C_I}(\mathbf{u}) - \mathbf{p} = \mathbf{0}, \\ \mathbf{p} \geq \mathbf{0}. \end{cases} \end{aligned} \tag{4.4}$$

Applying KKT formulation [16] to (4.4), the optimality conditions can be expressed as follows,

$$\begin{gathered}\mathbf{Gu}+\mathbf{c}+\mathbf{A}_{\mathbf{I}}^{\mathbf{T}}\boldsymbol{\lambda}=\mathbf{0},\qquad \mathbf{A}_{\mathbf{I}}(\mathbf{u})=-\nabla\mathbf{C}_{\mathbf{I}}(\mathbf{u}),\qquad \mathbf{C}_{\mathbf{I}}(\mathbf{u})-\mathbf{p}=\mathbf{0},\\ \mathbf{P}\boldsymbol{\lambda}-\eta\mathbf{e}=\mathbf{0},\qquad \mathbf{e}=[1\ 1\ 1\ 1]^{T},\ \mathbf{p}>0,\ \boldsymbol{\lambda}>0,\end{gathered}\tag{4.5}$$

where $\boldsymbol{\lambda}$ is the vector of Lagrange multipliers and $\mathbf{P}$ is a $4\times 4$ diagonal matrix whose diagonal elements are the components of the vector $\mathbf{p}$.

### 4.2. Primal-Dual Path-Following Method Steps

The Primal-dual path-following IP method steps for IVDC are as follows:

*(1) Newton's Step Direction*

In each iteration, the step direction $\{\boldsymbol{\Delta}\mathbf{p},\boldsymbol{\Delta}\mathbf{u},\boldsymbol{\Delta}\boldsymbol{\lambda}\}$ is obtained by applying Newton's method to KKT conditions (4.5):

$$\begin{aligned}\mathbf{r_c}+(\mathbf{G}+\boldsymbol{\Lambda}_{\mathbf{2}})\boldsymbol{\Delta}\mathbf{u}+\mathbf{A}_{\mathbf{I}}^{\mathbf{T}}\boldsymbol{\Delta}\boldsymbol{\lambda}&=\mathbf{0},\\ \mathbf{r_b}-\mathbf{A_I}\boldsymbol{\Delta}\mathbf{u}-\boldsymbol{\Delta}\mathbf{p}&=\mathbf{0},\\ \mathbf{r_s}+\mathbf{P}\boldsymbol{\Delta}\boldsymbol{\lambda}+\boldsymbol{\Lambda}\boldsymbol{\Delta}\mathbf{p}&=\mathbf{0},\end{aligned}\tag{4.6}$$

where the residuals $\mathbf{r_c}$, $r_{\mathbf{b}}$, and $r_{\mathbf{s}}$ are obtained as

$$\mathbf{r_c}=\mathbf{Gu}+\mathbf{c}+\mathbf{A}_{\mathbf{I}}^{T}\boldsymbol{\lambda},\qquad \mathbf{r_b}=\mathbf{C_I}(\mathbf{u})-\mathbf{p},\qquad \mathbf{r_s}=\mathbf{P}\boldsymbol{\lambda}-\eta\mathbf{e},\tag{4.7}$$

$$\mathbf{P}=\operatorname{diag}(p_1,p_2,p_3,p_4),\qquad \boldsymbol{\Lambda}=\operatorname{diag}(\lambda_1,\lambda_2,\lambda_3,\lambda_4),\qquad \boldsymbol{\Lambda}_{\mathbf{2}}=2\operatorname{diag}(\boldsymbol{\Lambda},\boldsymbol{\Lambda}).\tag{4.8}$$

Equation (4.6) is solved to achieve the step directions

$$\begin{aligned}\boldsymbol{\Delta}\mathbf{u}&=\left(\mathbf{G}+\boldsymbol{\Lambda}_{\mathbf{2}}+\mathbf{A}_{\mathbf{I}}^{\mathbf{T}}\mathbf{P}^{-\mathbf{1}}\boldsymbol{\Lambda}\mathbf{A}_{\mathbf{I}}\right)^{-1}\left(\mathbf{A}_{\mathbf{I}}^{\mathbf{T}}\mathbf{P}^{-1}(\mathbf{r_s}+\boldsymbol{\Lambda}\mathbf{r_b})-\mathbf{r_c}\right),\\ \boldsymbol{\Delta}\boldsymbol{\lambda}&=-\mathbf{P}^{-1}(\mathbf{r_s}+\boldsymbol{\Lambda}\mathbf{r_b})+\mathbf{P}^{-1}\boldsymbol{\Lambda}\mathbf{A_I}\boldsymbol{\Delta}\mathbf{u},\\ \boldsymbol{\Delta}\mathbf{p}&=\mathbf{r_b}-\mathbf{A_I}\boldsymbol{\Delta}\mathbf{u}.\end{aligned}\tag{4.9}$$

*(2) Step Length Calculation*

To satisfy nonnegativity condition $(\mathbf{p},\boldsymbol{\lambda})\geq\mathbf{0}$, the new iteration $(\mathbf{u}^{+},\mathbf{p}^{+},\boldsymbol{\lambda}^{+})$ is calculated as

$$\mathbf{u}^{+}=\mathbf{u}+\alpha_s^{\max}\Delta\mathbf{u},\qquad \mathbf{p}^{+}=\mathbf{p}+\alpha_s^{\max}\boldsymbol{\Delta}\mathbf{p},\qquad \boldsymbol{\lambda}^{+}=\boldsymbol{\lambda}+\alpha_{\lambda}^{\max}\boldsymbol{\Delta}\boldsymbol{\lambda},\tag{4.10}$$

where

$$\begin{aligned}\alpha_s^{\max} &= \max\{\alpha\epsilon(0,1] : \mathbf{p} + \alpha\Delta\mathbf{p} \geq (1-\tau)\mathbf{p}\}, \quad \tau\ \epsilon\ (0,1),\\ \alpha_\lambda^{\max} &= \max\{\alpha\epsilon(0,1] : \boldsymbol{\lambda} + \alpha\Delta\boldsymbol{\lambda}\ \geq (1-\tau)\boldsymbol{\lambda}\}.\end{aligned} \tag{4.11}$$

*(3) Updating the Barrier Parameter* $\eta$

The sequence of barrier parameters $\{\boldsymbol{\eta}_\mathbf{k}\}$ converges to zero by the update law

$$\eta_{k+1} = \sigma_k \frac{\mathbf{p}_\mathbf{k}^\mathbf{T}\boldsymbol{\lambda}_\mathbf{k}}{\mathbf{4}}, \quad \sigma_k\epsilon[0,1], \tag{4.12}$$

where to update the centring parameter $\sigma_k$, first, the predictor (affine scaling) direction $\{\Delta\mathbf{u}^{\text{aff}}, \Delta\mathbf{p}^{\text{aff}}, \Delta\boldsymbol{\lambda}^{\text{aff}}\}$ and the corresponding longest step lengths $\alpha_s^{\text{aff}}$ and $\alpha_\lambda^{\text{aff}}$ are calculated by setting $\eta = 0$ in (4.9) and (4.11). Then the value of complementarity along the affine scaling $\eta_{\text{aff}}$ step is defined to be

$$\eta_{\text{aff}} = \left(\mathbf{p}_\mathbf{k} + \alpha_s^{\text{aff}}\Delta\mathbf{p}^{\text{aff}}\right)^T\left(\boldsymbol{\lambda}_\mathbf{k} + \alpha_\lambda^{\text{aff}}\Delta\boldsymbol{\lambda}^{\text{aff}}\right). \tag{4.13}$$

The centring parameter is updated as follows:

$$\sigma_k = \left(\frac{\eta_{\text{aff}}}{\mathbf{p}_\mathbf{k}^\mathbf{T}\boldsymbol{\lambda}_\mathbf{k}/\mathbf{4}}\right)^3. \tag{4.14}$$

*(4) Stopping Criteria*

The algorithm is terminated, when the following error function with $\eta = 0$ has converged sufficiently close to zero

$$E(\mathbf{u},\mathbf{p},\boldsymbol{\lambda},\eta) = \max\left\{\left\|\mathbf{G}\mathbf{u} + \mathbf{c} + \mathbf{A}_\mathbf{I}^T\boldsymbol{\lambda}\right\|,\ \|\mathbf{C}_\mathbf{I}(\mathbf{u}) - \mathbf{p}\|,\ \left\|\mathbf{P}\boldsymbol{\lambda} - \eta\mathbf{e}\right\|\right\}. \tag{4.15}$$

All of these steps have been summarized in Pseudocode 1. To reduce the time of control allocation, the last allocated $\mathbf{u}$ is chosen as the initial value of the control input $\mathbf{u_0}$. Then, $\mathbf{u_0}$ is modified (reduced) to satisfy tire saturation constraints.

## 5. Dynamic Control Allocation

DCA uses an optimizing update law for system inputs. Since it is not required to solve the optimization problem at each sampling time, the main advantage of DCA is its computational efficiency. In what follows, the procedure explained in [8] is applied to the proposed integrated vehicle control scheme. However, the interested reader might refer to [8, 9] for convergence study and detailed analysis.

**Given** $A$, $W$ , and $v$
  Compute $\mathbf{G}$, $\mathbf{c}$, and $\mathbf{h}$ in (4.2).
  Choose the allocated control input of the previous sample time as the initial value $\mathbf{u_0}$
  If each entry of $\mathbf{u_0}$ violates the inequality (3.9), reduce it to satisfy (3.9)
  Compute initial values for $\mathbf{p}_0$ and $\boldsymbol{\lambda}_0$.
  Compute the initial value for barrier parameter $\eta$.
  Compute residuals $\mathbf{r_c}$, $\mathbf{r_b}$, and $\mathbf{r_s}$ given in(4.7)
  Select error tolerance $\varepsilon$ and set $k \leftarrow 0$.
**repeat** until $E(\mathbf{u}, \mathbf{p}, \boldsymbol{\lambda}, 0) \leq \varepsilon$
  Compute step direction from equation (4.9),
  Compute step size to satisfy nonnegativity conditions using (4.11),
  Update the variables $\mathbf{u}$, $\mathbf{p}$, and $\boldsymbol{\lambda}$ using (4.10),
  Compute affine scaling $\eta_{\text{aff}}$ step from (4.13) and $\sigma_k$ according to (4.14),
  Update the barrier parameter $\eta_{k+1}$ based on (4.12),
  Compute residuals $\mathbf{r_c}$, $\mathbf{r_b}$, and $\mathbf{r_s}$ from (4.7),
  Set $k \leftarrow k + 1$
**end**

**PSEUDOCODE 1:** Pseudocode for interior-point algorithm.

### *5.1. Dynamic Control Allocation Applied to IVDC*

DCA is formulated by introducing the following Lagrangian based on (3.13):

$$\ell = \mathbf{u}^{\mathbf{T}}\mathbf{W}\mathbf{u} + (\mathbf{v} - \mathbf{A}\mathbf{u})^{\mathbf{T}}\boldsymbol{\lambda}_{\text{dyn}} - \omega_{\text{dyn}}\sum_{i=1}^{4}\log(C_{Ii}(u_i, u_{i+4})) \tag{5.1}$$

with $\omega_{\text{dyn}} > 0$ and $\boldsymbol{\lambda}_{\text{dyn}}$ being a 3-component vector of Lagrange multipliers. DCA updates $\mathbf{u}$ and $\boldsymbol{\lambda}_{\text{dyn}}$ in the form of the Newton-like update law

$$\begin{bmatrix} \dot{\mathbf{u}} \\ \dot{\boldsymbol{\lambda}}_{\text{dyn}} \end{bmatrix} = -\gamma_{\text{dyn}}\left(\mathbb{H}^{T}\mathbb{H} + \varepsilon_{\text{dyn}}\mathbf{I}\right)^{-1}\mathbb{H}\begin{bmatrix} \dfrac{\partial \ell}{\partial \mathbf{u}} \\ \dfrac{\partial \ell}{\partial \boldsymbol{\lambda}_{\text{dyn}}} \end{bmatrix} + \begin{bmatrix} \boldsymbol{\zeta} \\ \boldsymbol{\phi} \end{bmatrix}, \tag{5.2}$$

where $\gamma_{\text{dyn}} > 0$ and $\varepsilon_{\text{dyn}} \geq 0$, and for our problem $\mathbb{H}$ is written as

$$\mathbb{H} = \begin{bmatrix} \dfrac{\partial^2 \ell}{\partial \mathbf{u}^2} & -\dfrac{\partial(\mathbf{A}\mathbf{u})^{\mathbf{T}}}{\partial \mathbf{u}} \\ -\dfrac{\partial(\mathbf{A}\mathbf{u})}{\partial \mathbf{u}} & \mathbf{0} \end{bmatrix}. \tag{5.3}$$

In (5.2) the feedforward-like terms $\boldsymbol{\zeta}$ and $\boldsymbol{\phi}$ are chosen so that the following scalar algebraic equation holds:

$$\boldsymbol{\alpha}_{\text{dyn}}^{\mathbf{T}}\boldsymbol{\zeta} + \boldsymbol{\beta}_{\text{dyn}}^{\mathbf{T}}\boldsymbol{\phi} + \delta_{\text{dyn}} = 0 \tag{5.4}$$

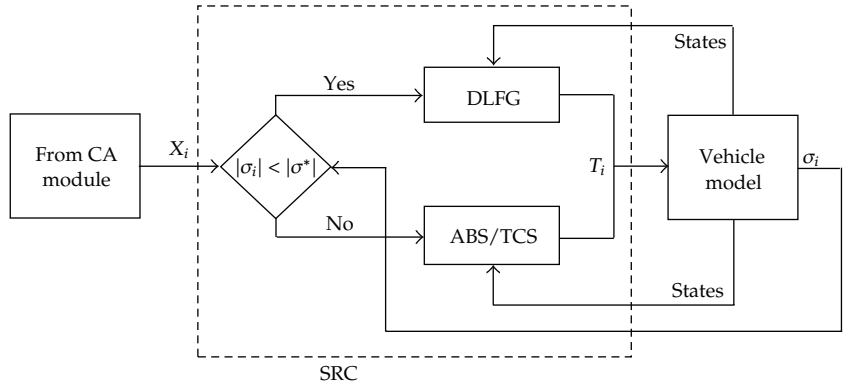


**Figure 3:** The SRC scheme applied to the vehicle system.

with

$$\begin{bmatrix} \boldsymbol{\alpha}_{\text{dyn}} \\ \boldsymbol{\beta}_{\text{dyn}} \end{bmatrix} = \mathbb{H} \begin{bmatrix} \dfrac{\partial \ell}{\partial \mathbf{u}} \\ \dfrac{\partial \ell}{\partial \boldsymbol{\lambda}_{\text{dyn}}} \end{bmatrix}, \qquad \delta_{\text{dyn}} = -(\mathbf{A}\mathbf{u} - \mathbf{v})^T \dot{\mathbf{v}}. \tag{5.5}$$

Assume that the stability of the high-level control could be shown through a Lyapunov function $V_0(t, r, \beta)$, then, by the Lyapunov function

$$V_{\text{dyn}}(t, r, \beta, \mathbf{u}, \boldsymbol{\lambda}_{\text{dyn}}) = \sigma_{\text{dyn}} V_0(t, r, \beta) + \frac{1}{2}\left( \frac{\partial \ell^T}{\partial \mathbf{u}} \frac{\partial \ell}{\partial \mathbf{u}} + \frac{\partial \ell^T}{\partial \boldsymbol{\lambda}_{\text{dyn}}} \frac{\partial \ell}{\partial \boldsymbol{\lambda}_{\text{dyn}}} \right), \quad \sigma_{\text{dyn}} > 0, \tag{5.6}$$

global exponential convergence to optimality conditions is achieved.

### 5.2. Discussion and Modification

Consider the equality-constrained optimization problem with the Lagrangian (5.1). Then the optimizing conditions are

$$\begin{bmatrix} \dfrac{\partial \ell}{\partial \mathbf{u}} \\ \dfrac{\partial \ell}{\partial \boldsymbol{\lambda}_{\text{dyn}}} \end{bmatrix} = \mathbf{0}. \tag{5.7}$$

Applying Newton's conditions to (5.7) results in optimizing Newton's steps $\Delta\mathbf{u}$ and $\Delta\boldsymbol{\lambda}_{\text{dyn}}$

$$\begin{bmatrix} \dfrac{\partial^2 \ell}{\partial \mathbf{u}^2} & \dfrac{\partial}{\partial \boldsymbol{\lambda}_{\text{dyn}}} \left( \dfrac{\partial \ell}{\partial \mathbf{u}} \right)^T \\ \dfrac{\partial}{\partial \mathbf{u}} \left( \dfrac{\partial \ell}{\partial \boldsymbol{\lambda}_{\text{dyn}}} \right) & \dfrac{\partial^2 \ell}{\partial \boldsymbol{\lambda}_{\text{dyn}}^2} \end{bmatrix} \begin{bmatrix} \Delta\mathbf{u} \\ \Delta\boldsymbol{\lambda}_{\text{dyn}} \end{bmatrix} = - \begin{bmatrix} \dfrac{\partial \ell}{\partial \mathbf{u}} \\ \dfrac{\partial \ell}{\partial \boldsymbol{\lambda}_{\text{dyn}}} \end{bmatrix} \tag{5.8}$$

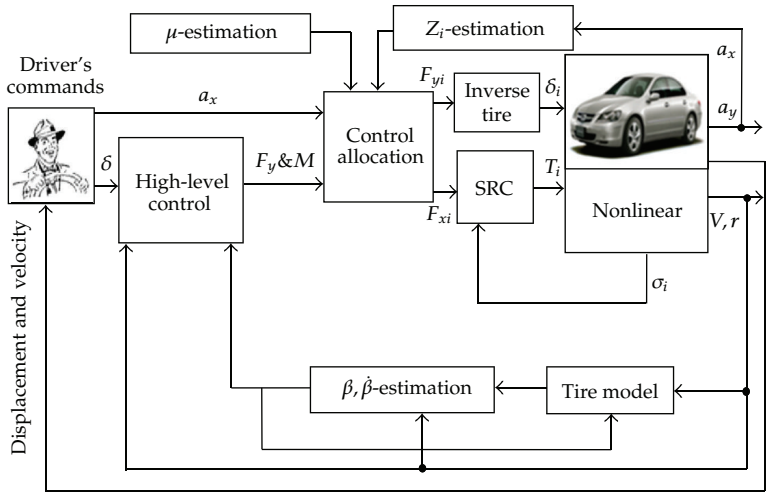


**Figure 4:** Overall closed loop scheme of the proposed IVDC.

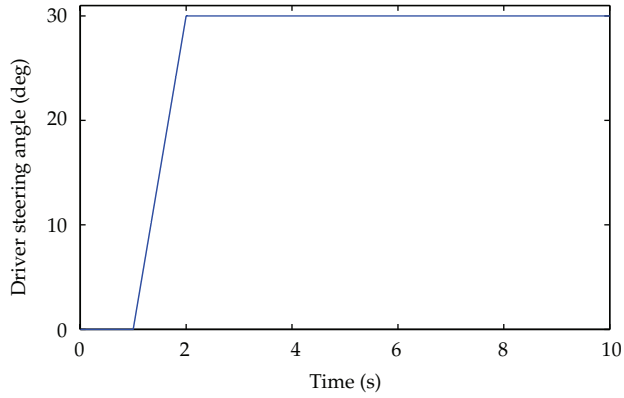


**Figure 5:** Driver steering command in split-$\mu$ scenario.

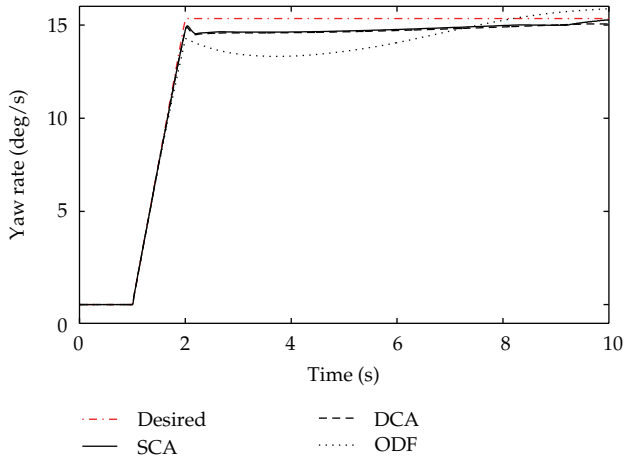


**Figure 6:** Yaw angle velocity in split-$\mu$ scenario.

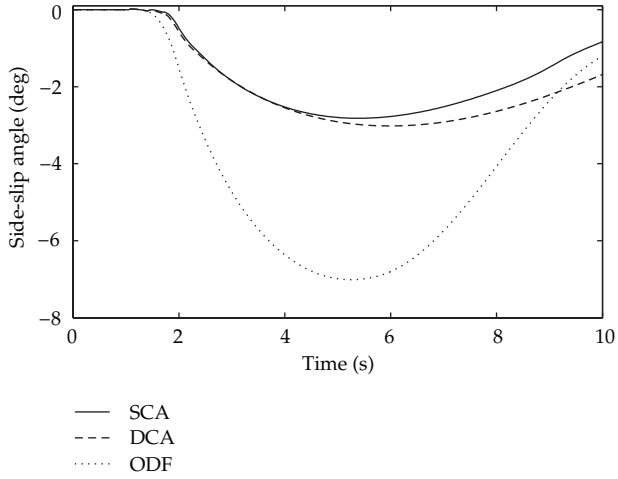


**Figure 7:** Side-slip angle in split-$\mu$ scenario.

or

$$\begin{bmatrix} \Delta \mathbf{u} \\ \Delta \boldsymbol{\lambda}_{\text{dyn}} \end{bmatrix} = \begin{bmatrix} \dfrac{\partial^2 \ell}{\partial \mathbf{u}^2} & -\dfrac{\partial (\mathbf{A}\mathbf{u})^T}{\partial \mathbf{u}} \\ -\dfrac{\partial (\mathbf{A}\mathbf{u})}{\partial \mathbf{u}} & \mathbf{0} \end{bmatrix}^{-1} \begin{bmatrix} \dfrac{\partial \ell}{\partial \mathbf{u}} \\ \dfrac{\partial \ell}{\partial \boldsymbol{\lambda}_{\text{dyn}}} \end{bmatrix} = \mathbb{H}^{-1} \begin{bmatrix} \dfrac{\partial \ell}{\partial \mathbf{u}} \\ \dfrac{\partial \ell}{\partial \boldsymbol{\lambda}_{\text{dyn}}} \end{bmatrix}. \tag{5.9}$$

By setting $\varepsilon_{\text{dyn}} = 0$, ignoring the terms $\boldsymbol{\zeta}$ and $\boldsymbol{\phi}$, and considering the symmetry of $\mathbb{H}$, it can be demonstrated that the update law (5.2) represents the solution of $\Delta \mathbf{u}$ and $\Delta \boldsymbol{\lambda}_{\text{dyn}}$ in (5.9), that is, one Newton's step towards the optimum point. Therefore, (5.9) can be interpreted as one Newton's step from the solution of the control allocation problem at the current sampling time for the solution at the next instant, for which the terms $\boldsymbol{\zeta}$ and $\boldsymbol{\phi}$ are to compensate time-varying optimum solution.

Despite the log-barrier term in (5.1), depending on the values of $\gamma_{\text{dyn}}$ and $\omega_{\text{dyn}}$, there is no guarantee that the Newton-like step (5.2) will satisfy the inequality constraints (3.9). As the $i$th inequality constraint is infringed, $C_{Ii}$ becomes negative and $\log(C_{Ii})$ and correspondingly the Lagrangian (5.1) turn meaningless. To tackle this problem, in this paper, a line search is adopted for the coefficient $\gamma_{\text{dyn}}$, so that the resulting $\mathbf{u}$ and $\boldsymbol{\lambda}_{\text{dyn}}$ at the next sampling time satisfy the inequality constraints $\mathbf{C_I} > \mathbf{0}$ and $\boldsymbol{\lambda}_{\text{dyn}} > 0$. The idea of the line search approach is taken from the second step of the interior-point stages, described in the previous section.

Another problem with DCA is that (5.2) could induce a Newton's step from an infeasible point, violating the inequality constraints (3.9), because of time-varying nature of these constraints. This arises because the term $(\mu_i Z_i)^2$ in (3.9) is time varying. Consequently, it is possible for the feasible solution at the current time to violate the inequality constraints of the next sample time. In such conditions, (5.2) needs to be modified for Newton's steps from infeasible points [15].

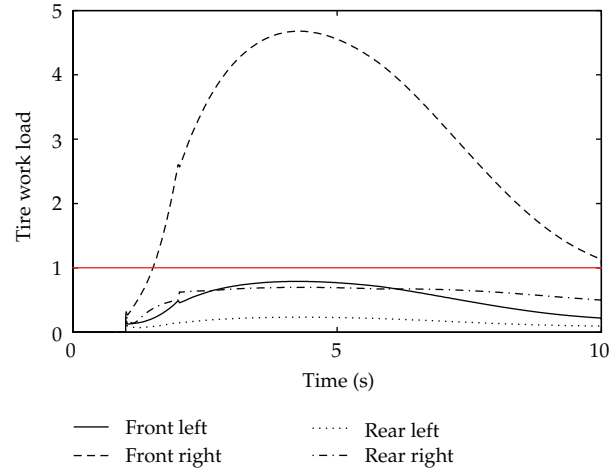


**Figure 8:** Tire work-load distribution by ODF in split-$\mu$ scenario.

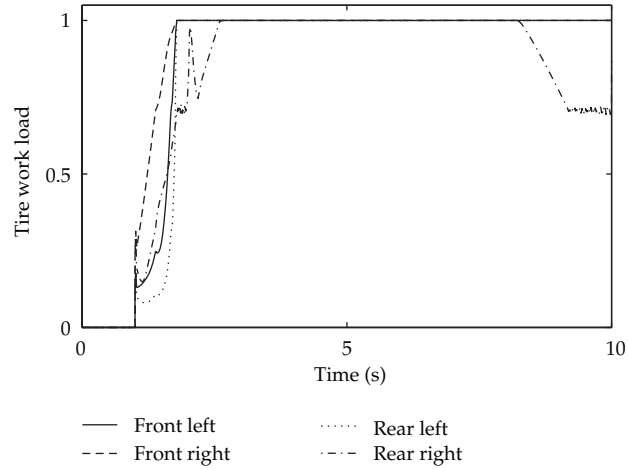


**Figure 9:** Tire work-load distribution by SCA in split-$\mu$ scenario.

After desired longitudinal and lateral forces of each tire are computed by either of the proposed control allocation algorithms, the active steering angle, $\delta_i$, at wheel $i$ can be determined as follows:

$$\begin{aligned} \delta_i &\approx \beta + \frac{L_f r}{v_{xi}} - \alpha_i, \quad i = 1,2, \\ \delta_i &\approx \beta - \frac{L_r r}{v_{xi}} - \alpha_i, \quad i = 3,4, \end{aligned} \tag{5.10}$$

where $v_{xi}$ is the longitudinal velocity of the $i$th tire and $\alpha_i$ is the side-slip angle of the $i$th tire and is obtained using the inverse of a simple tire model as

$$\alpha_i = \begin{cases} -\dfrac{Y_i}{C_i}, & X_i^2 + Y_i^2 \le n * \left(\mu_i Z_i\right)^2, \quad 0 < n < 1, \\ -\mu_i Z_i * \arctan\left(\dfrac{K_i Y_i}{\mu_i Z_i C_i}\right), & X_i^2 + Y_i^2 > n * \left(\mu_i Z_i\right)^2, \quad i = 1, \ldots, 4, \end{cases} \tag{5.11}$$

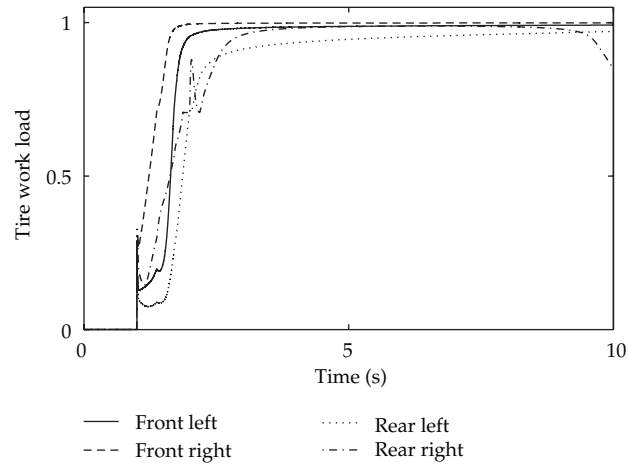


**Figure 10:** Tire work-load distribution by DCA in split-$\mu$ scenario.

in which $C_i$ denotes the cornering stiffness of the $i$th tire and $K_i$s are chosen to approximate the saturation conditions. Longitudinal forces are fed into the low-level control unit.

## 6. Low-Level Slip-Ratio Control Design

The longitudinal force of each tire is related to the corresponding longitudinal slip ratio and is adjusted through slip-ratio control (SRC). The slip ratio of the $i$th tire, $\sigma_i$, is defined as

$$\sigma_i = \frac{R\omega_i - v_{xi}}{v_{xi}} \quad \text{during braking,} \tag{6.1}$$

$$\sigma_i = \frac{R\omega_i - v_{xi}}{R\omega_i} \quad \text{during acceleration,} \tag{6.2}$$

where $R$ denotes the radius and $\omega_i$ is the angular velocity of the $i$th wheel. In the case where longitudinal slip ratio is small, the longitudinal tire force is found to be proportional to the slip ratio. Then, it gains its maximum value at a typical value of $\sigma^*$, after which it starts to lessen. Experimental studies have established that the tire lateral force decreases with increasing slip ratios greater than $|\sigma^*|$ as well [17].

### *6.1. Description of the SRC Scheme*

In this paper, when the tire slip ratio is smaller than $\sigma^*$, by neglecting the wheel rotational inertia [3], the applied braking/traction torque, $T_i$, at wheel $i$ is obtained as

$$T_i = RX_i. \tag{6.3}$$

In this case, the SRC works for Desired Longitudinal Force Generation (DLFG). However, when the demanded $X_i$ is too high, applying (6.3) would increase the slip ratio beyond $\sigma^*$,

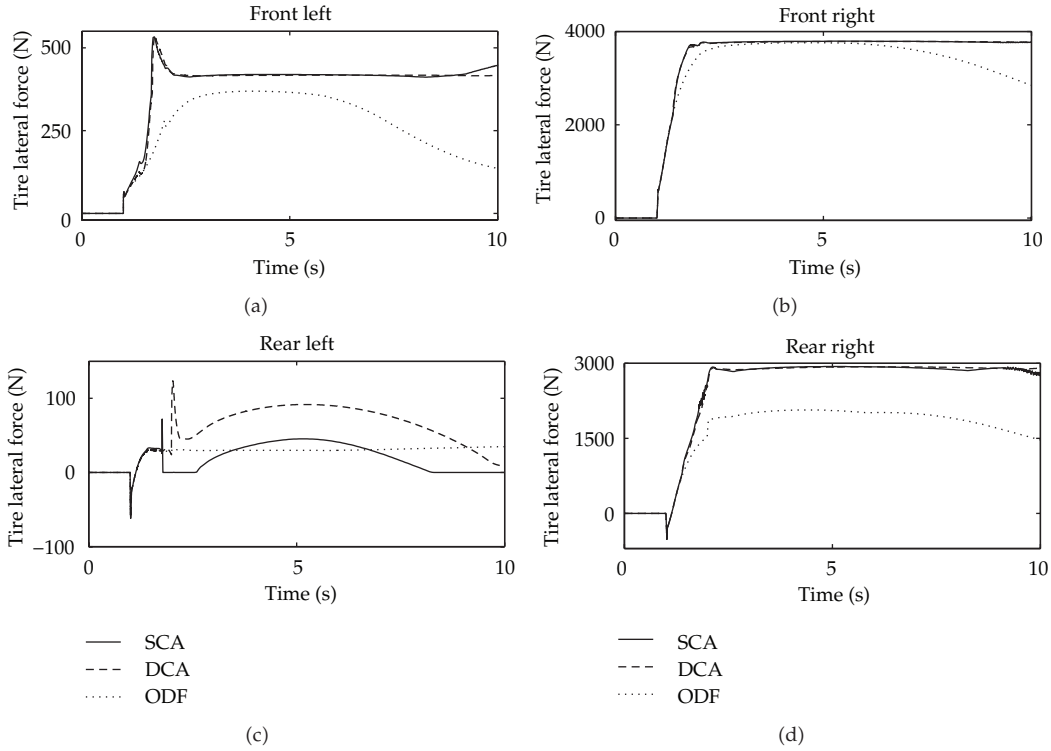


**Figure 11:** Actually generated tire lateral forces in split-$\mu$ scenario.

inevitably leading to wheel lock and lateral tire force drop. In such conditions, the idea of Antilock Braking System (ABS) is employed to keep the slip ratio of tires at $\sigma^*$. This idea is utilized during both braking and traction. When traction torque applies, the proposed slip-ratio control is in the Traction Control System (TCS) mode. The SRC scheme is shown in Figure 3.

### *6.2. The ABS/TCS Design*

The $i$th wheel rotational dynamics is stated as

$$I_\omega \dot{\omega}_i = T_i - RF_{x_i}, \tag{6.4}$$

where $I_\omega$ is wheel rotational inertia. To achieve slip-ratio differential equation when braking, by differentiating (6.1) and replacing for $\dot{\omega}_i$ from (6.4)

$$\dot{\sigma}_i = \frac{R}{I_\omega v_{xi}}(T_i - rF_{x_i}) - (1+\sigma_i)\frac{\dot{v}_{xi}}{v_{xi}}. \tag{6.5}$$

During decelerating, the longitudinal force can be stated as [17]

$$F_{x_i} = C_\sigma \sigma_i + \Delta F_{x_i} \tag{6.6}$$

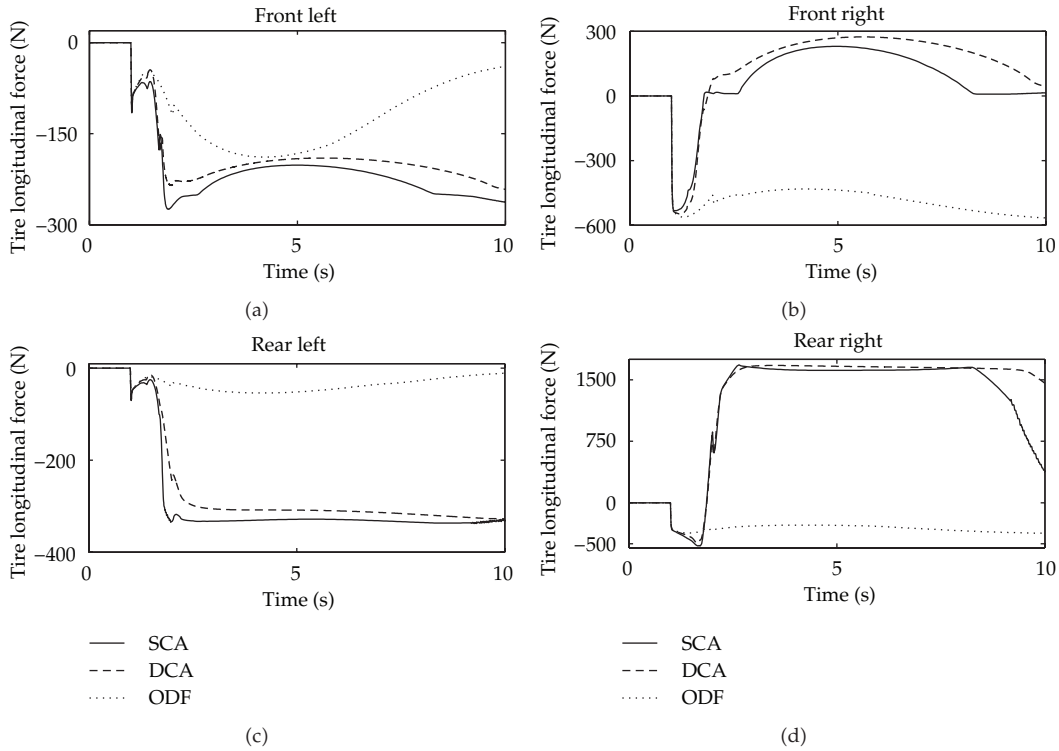


**Figure 12:** Actually generated tire longitudinal forces in split-$\mu$ scenario.

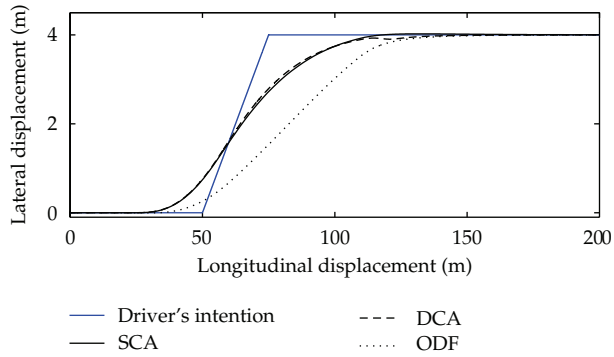


**Figure 13:** Vehicle path in SLC.

in which the term $C_\sigma \sigma_i$ represents the linear part, with $C_\sigma$ being the tire longitudinal stiffness, and $\Delta F_{x_i}$ is the deviation from the linear part and is bounded by $\overline{F}_{x_i}$:

$$0 < \Delta F_{x_i} < \overline{F}_{x_i}. \tag{6.7}$$

The goal of the ABS is to regulate $\sigma_i$ around the constant value $\sigma^*$. Applying the sliding mode control design procedure to (6.5), an ABS is designed so that to get the sliding condition

$$\frac{d}{dt}\frac{1}{2}s_\sigma^2 \leq -\eta_\sigma |s_\sigma|, \quad s_\sigma = \sigma_i - \sigma^*, \ \sigma^* < 0, \ \eta_\sigma > 0, \tag{6.8}$$

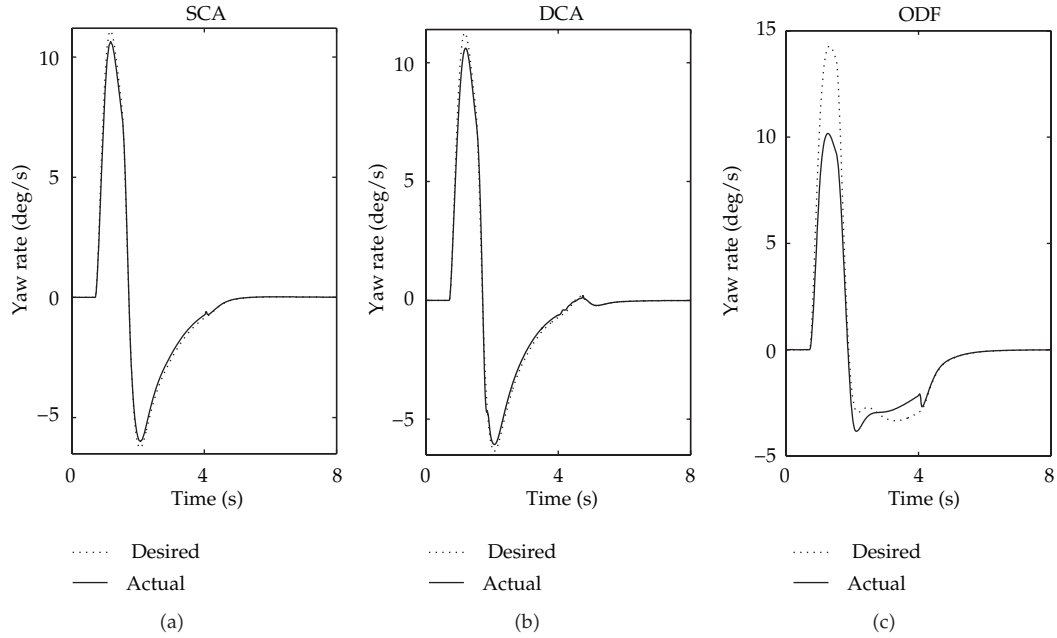


**Figure 14:** Yaw rate in SLC.

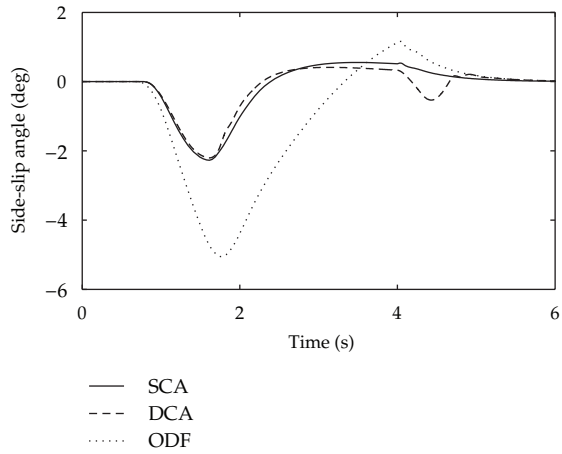


**Figure 15:** Side-slip angle in SLC.

the applied braking torque at the $i$th wheel is

$$T_i = RC_\sigma \sigma^* + \frac{I_\omega \dot{v}_{xi}}{R}(1+\sigma_i) - \frac{I_\omega v_{xi}}{R} k_\sigma \operatorname{sat}\left(\frac{s_\sigma}{\phi_\sigma}\right), \quad k_\sigma > \frac{R^2}{I_\omega v_{xi}} \overline{F}_{x_i} + \eta_\sigma,\ \phi_\sigma > 0. \tag{6.9}$$

Furthermore, the applied torque during acceleration, by TCS, is computed as

$$T_i = RC_\sigma |\sigma^*| + \frac{I_\omega \dot{v}_{xi}}{R(1-\sigma_i)} - \frac{I_\omega v_{xi}}{R(1-\sigma_i)^2} k_\sigma \operatorname{sat}\left(\frac{s_\sigma}{\phi_\sigma}\right), \quad s_\sigma = \sigma_i - |\sigma^*|. \tag{6.10}$$

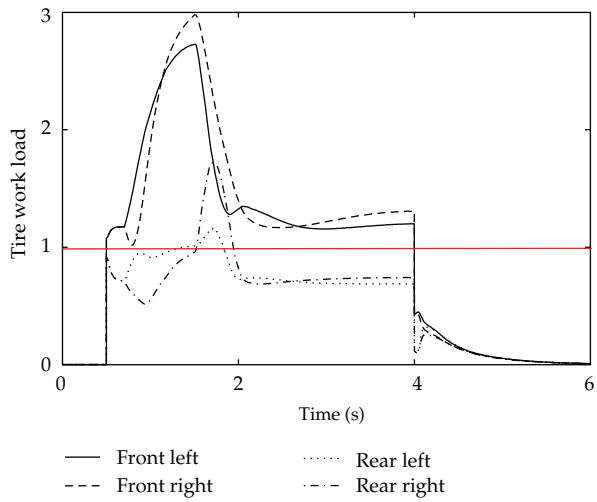


**Figure 16:** Work-load distribution by ODF in SLC.

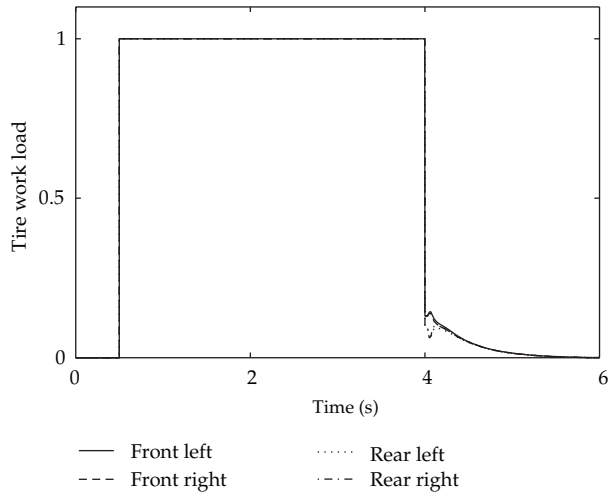


**Figure 17:** Tire work-load distribution by SCA in SLC.

## 7. Simulation Results

The considered methods are tested in several critical maneuvers. A 9DoF nonlinear vehicle model is used for simulation purpose [4]. The vehicle behavior is probed during an open-loop maneuver, with no driver model, and two closed-loop maneuvers, including the driver model validated experimentally in [18]. The overall control scheme for simulation is shown in Figure 4. Comparison is made with a well-recognized case [3], where tire saturation conditions are ignored in ODF.

The simulations are performed by MATLAB/Simulink. For the sake of practical implementations, the time for each control allocation was computed. Using a PC based on a 2.6 GHz Intel Core 2 Duo T9500 processor, the maximum time for the total IP algorithm

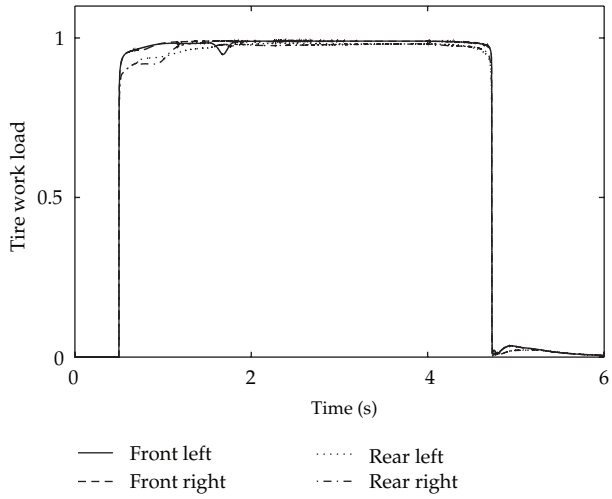


**Figure 18:** Tire work-load distribution by DCA in SLC.

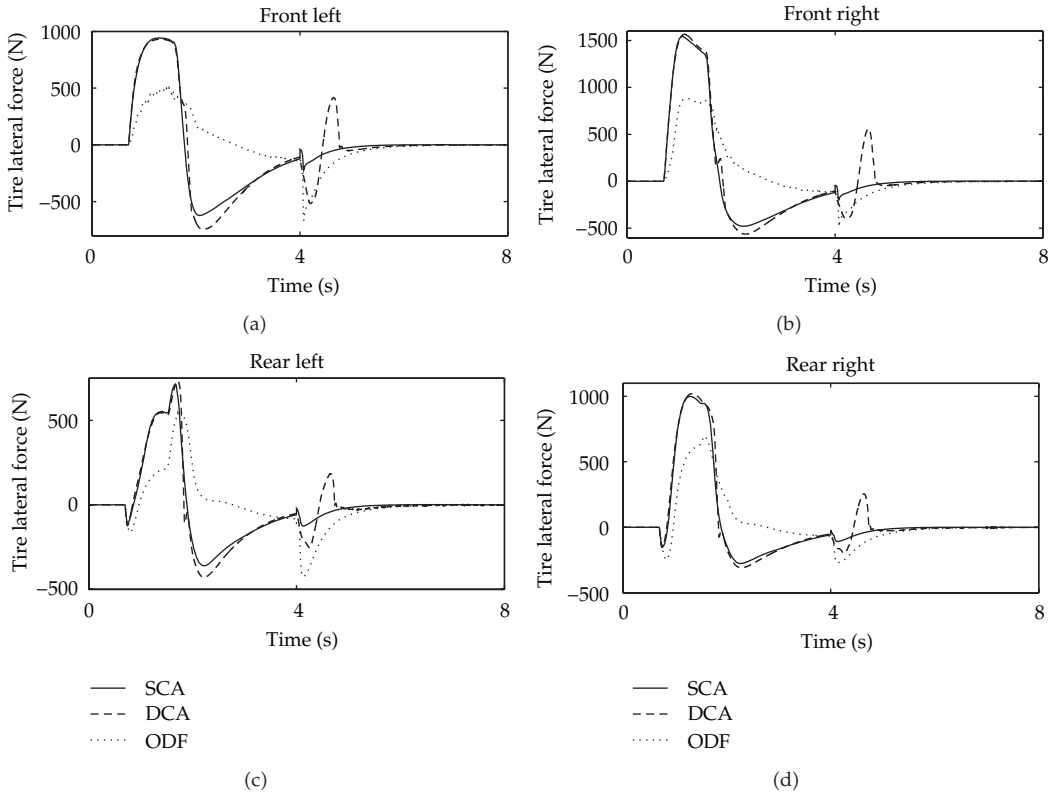


**Figure 19:** Actually generated tire lateral forces in SLC.

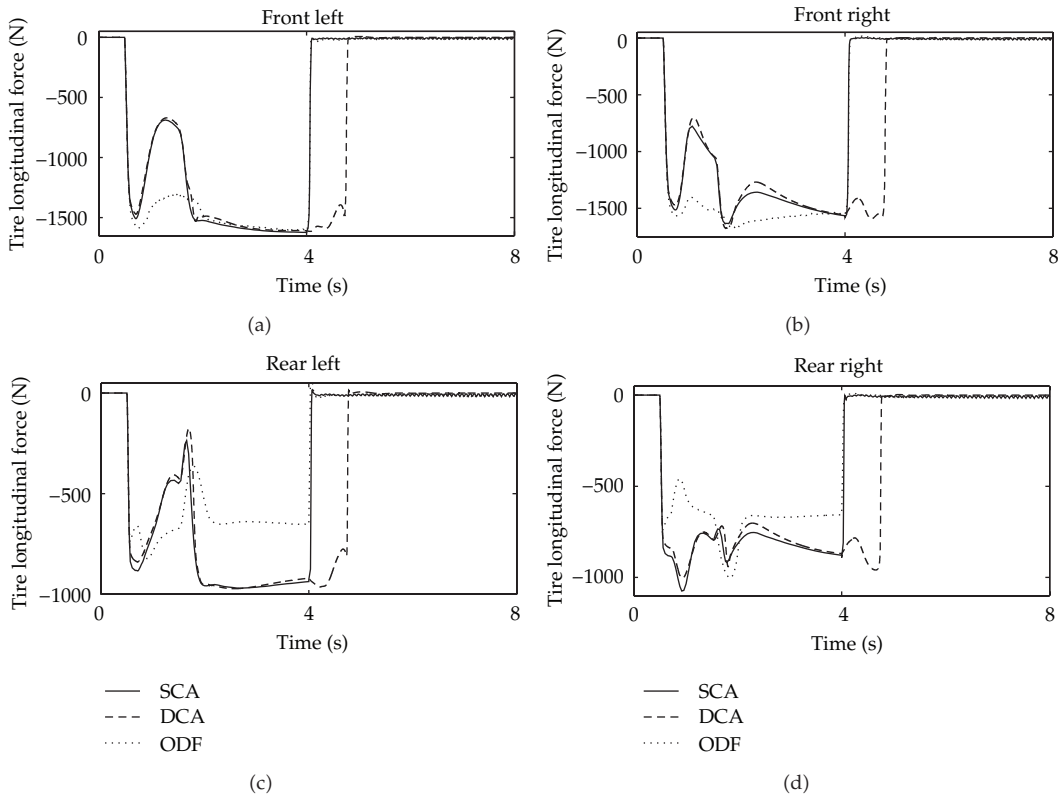


**Figure 20:** Actually generated tire longitudinal forces in SLC.

is about 0.002 seconds. This time can be still improved using efficient C-Programming and effective numerical techniques.

### *7.1. Open-Loop Cornering Maneuver on a Split-$\mu$ Road*

The vehicle behaviour is examined in an open-loop split-$\mu$ manoeuvre, where the tire-road friction coefficients on the vehicle left and right are equal to 0.3 and 1, respectively. The vehicle is assumed to move with a velocity of 110 km/hr and to turn according to the steering angle in Figure 5. The deceleration demand is −0.1 g. In Figures 6 and 7, both Saturation Constrained ODF (SCODF) approaches, that is, SCA and DCA, have better yaw rate tracking and side-slip angle reduction. Using ODF, the allocated work load to the front-right wheel is substantially beyond its actual capacity, other tires have still margin to saturation, as Figure 8 shows. On the other hand, from Figures 9 and 10 it is seen that SCODF methods have balanced the workload distribution and managed to use the total capacity of tire forces by saturating all tires in critical conditions. Accordingly, as shown in Figures 11 and 12, these methods have generated larger lateral and longitudinal forces, compared to ODF. To compare SCA and DCA, it is noted (Figure 7) that SCA has less side slip at some points relative to DCA. This arises because DCA has failed to completely saturate the tire on rear left in this case. Furthermore, Figures 11 and 12 reveal that lateral and longitudinal forces by DCA have properly converged to the optimal solution of SCA, with minor errors in some cases.

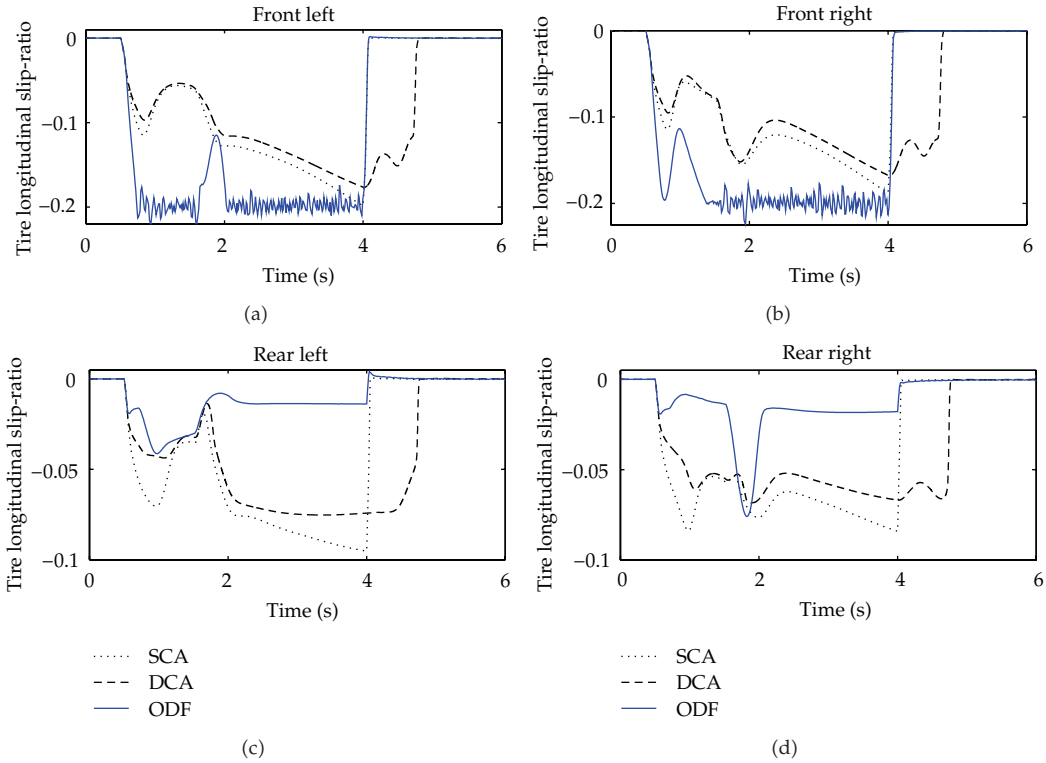


**Figure 21:** Tire longitudinal slip-ratios in SLC.

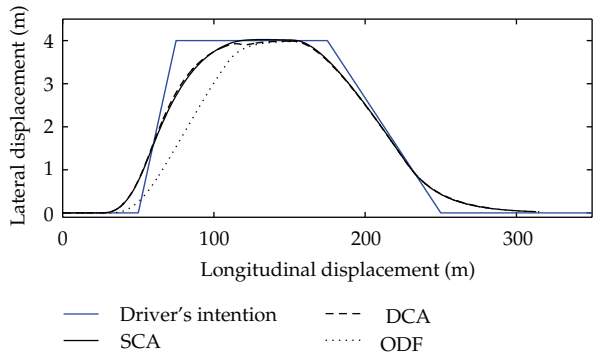


**Figure 22:** Vehicle path in DLC with $\mu = 0.5$.

## *7.2. Close-Loop Single-Lane Change Maneuver*

A closed-loop high-speed Single-Lane Changing (SLC) on a slippery road with the braking acceleration of $-0.5\,g$ is considered. The vehicle initial speed is 120 km/h and the tire-road friction coefficient is set at 0.5. By Figures 13, 14, 15, 16, 17, and 18, enhanced vehicle control in terms of vehicle trajectory, yaw rate, and side-slip angle, as well as balanced work load distribution by SCODF approaches are evident. Figure 19 illustrates that the generated tire lateral forces by ODF are smaller than SCODF approaches. For the tires at the vehicle rear, this is primarily due to the smaller work load assigned to these tires by ODF. However, reduction

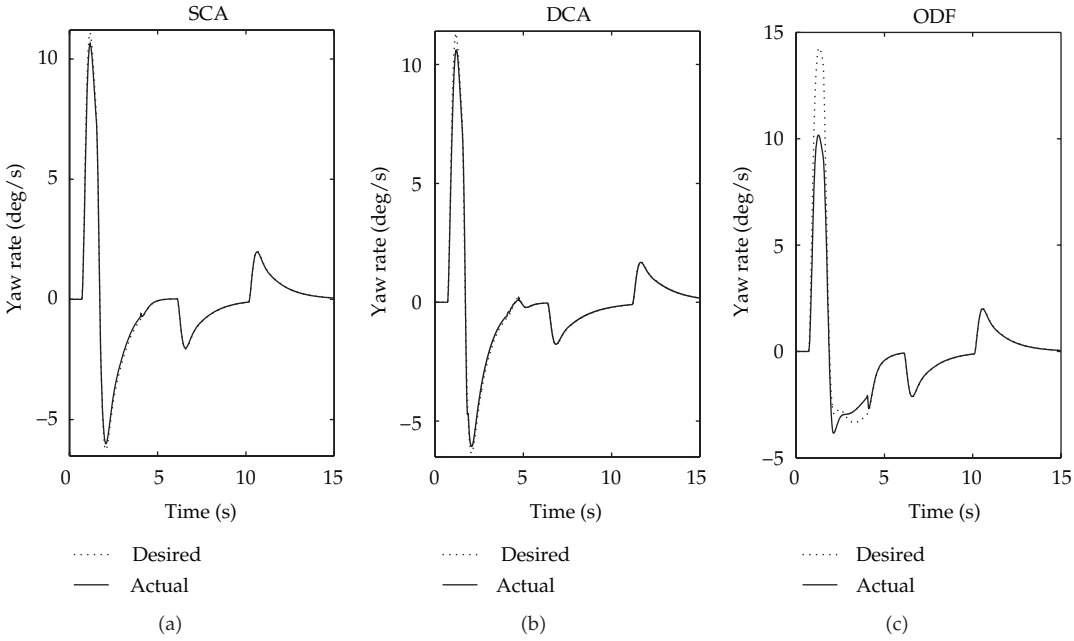


**Figure 23:** Yaw rate in DLC with $\mu = 0.5$.

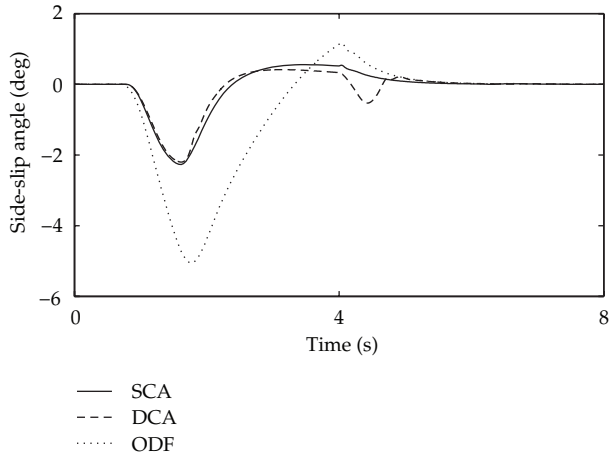


**Figure 24:** Side-slip angle in DLC with $\mu = 0.5$.

of the lateral forces at the front tires can be described referring to longitudinal forces and slip-ratio plots in Figures 20 and 21. The ODF method has designated larger braking forces to front tires at some points, compared with SCODF approaches. According to friction circle concept, this reduces the corresponding generated tire lateral forces by ODF. Accordingly, as Figure 21 demonstrates, higher longitudinal forces by ODF have increased the slip ratio of these wheels by $\sigma^* = 0.2$. Then, ABS is activated by SRC to regulate the front slip ratios at $\sigma^* = 0.2$. On the other hand, SCA and DCA moderate the role of longitudinal forces in vehicle control and leave out the use of ABS.

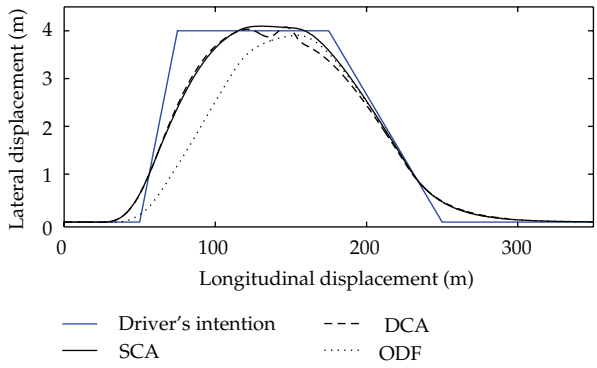


**Figure 25:** Vehicle path in DLC with $\mu = 0.4$.

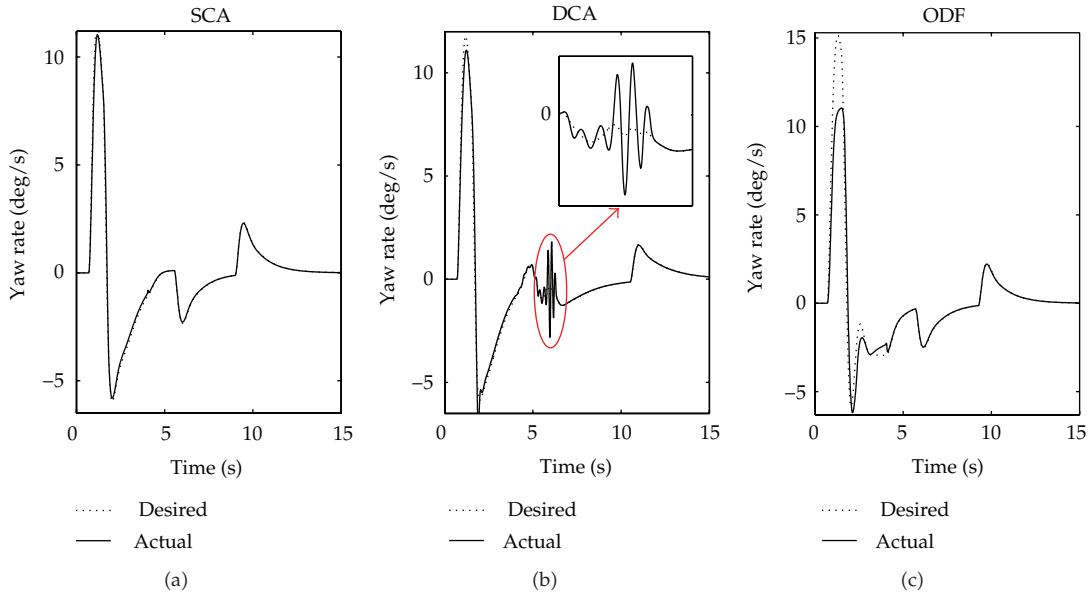


**Figure 26:** Yaw rate in DLC with $\mu = 0.4$.

### *7.3. Close-Loop Double-Lane Change Maneuver*

Another case to evaluate the system is high-speed Double-Lane Changing (DLC) on a slippery road with driver's braking. The maneuver conditions remain unchanged with respect to SLC. In Figures 22, 23, and 24, SCODF approaches are still superior in controlling the vehicle path, yaw rate, and side-slip angle.

To increase the challenge for the control systems, DLC is repeated on a more slippery road, where the tire-road friction coefficient is 0.4. Figures 25, 26, and 27 show the results in this case. Although both SCA and DCA methods have almost the same performance of vehicle control, oscillatory yaw rate response as well as more side-slip angle by DCA are clear. These are mainly due to transient response of DCA, specifically to panic reactions of driver in both steering and braking in critical conditions. The transient response is an inherent characteristic of the dynamic update law in DCA. In this scenario, the transient response

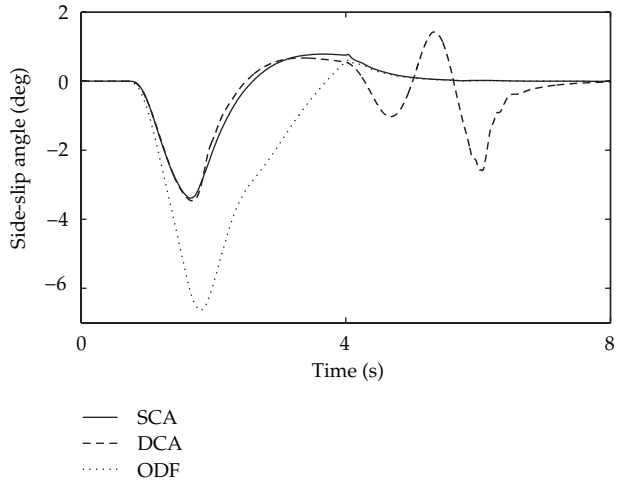


**Figure 27:** Side-slip angle in DLC with $\mu = 0.4$.

has been triggered when the DCA tries to compensate for sudden braking release demand by driver. Another reason for oscillatory response by DCA is its relatively low robustness against highly nonlinear characteristics of vehicle dynamics and tire forces which are more substantial in more critical conditions. The oscillations by DCA grow more considerable once sudden changes occur in tire/road friction coefficient, for example, when the vehicle suddenly enters an icy road. Oscillations can intensify also after an actuator fails in a specific manoeuvre, where DCA is used for actuator failure compensation, which is one of the main advantages of control allocation methods [1]. In general, oscillatory response by DCA increases as the manoeuvre conditions worsen.

## 8. Conclusion

Control allocation techniques can be applied effectively to enhance vehicle stability. Nonlinear vehicle motion control is split into three tasks. First, the total body lateral force and yaw moment were computed through a high-level sliding mode controller with adaptive upper bounds, where the knowledge of the upper bounds of uncertainties is not required. To allocate the vehicle high-level control objectives to saturation-constrained tire forces, static and dynamic control allocation techniques were formulated. Interior-point method was used to handle the nonlinear constrained optimization problem in SCA; a dynamic update law was derived using DCA. Simulation results were conducted, and vehicle operation under each method was evaluated and compared with a well-recognized work in the literature. It was seen that both SCA and DCA approaches manage to utilize whole capacity of tire forces more properly by offering *balanced work-load distribution* and *rational adjustment of longitudinal and lateral tire forces*. Since no optimization problem is required in DCA, the main advantage of this method is its computational efficiency for real-time implementations. Furthermore, although by DCA the set of distributed tire forces properly approaches the optimal one, that is, that of SCA, there is yet an amount of error, depending on the severity of maneuver. This error of DCA is mainly due to its transient response to panic behavior of driver and its relatively low robustness to highly nonlinear characteristics of vehicle dynamics and tire forces. Therefore, in maneuvers with more critical conditions, the performance of the vehicle control task can be degraded using DCA compared to SCA.

## Nomenclature

$a_x$: Driver's braking acceleration
$A_i$: Weighting coefficients of $i$th tire
$C_i$: Cornering stiffness of $i$th tire
$\mathbf{C_I}$: Vector of saturation constraints
$C_\sigma$: Tire longitudinal stiffness
$d$: Vehicle tread
$f$: Objective function
$F_{xi}$: Actual longitudinal force of $i$th tire
$\overline{\mathbf{F}}_{x_i}$: Maximum deviation from linear part for $F_{xi}$
$F_{yi}$: Actual lateral force of $i$th tire
$I_w$: Moment of inertia of each wheel
$I_z$: Yaw moment of inertia of vehicle
$\widehat{I}_z$: Estimation of yaw moment of inertia
$\widetilde{I}_z$: Estimation of yaw moment of inertia error
$\overline{I}_z$: Upper bound for $\widetilde{I}_z$
$J$: Objective function in quadratic form
$k_r$, $k_\beta$, $k_\sigma$: Sliding mode control gain
$\widehat{k}_{\beta 1}$, $\widehat{k}_{\beta 2}$, $\widehat{k}_{r1}$, $\widehat{k}_{r2}$: Adaptive gains
$k^d_{\beta 1}$, $k^d_{\beta 2}$, $k^d_{r1}$, $k^d_{r2}$: Uncertainty upper bound
$L$: Lagrangian
$L_{f,r}$: Distance between mass center and axle
$m$: Vehicle mass
$\widehat{m}$: Vehicle mass estimation
$\widetilde{m}$: Mass estimation error
$\overline{m}$: Upper bound for $\widetilde{m}$
$M$: Body yaw moment
$R$: Wheel radius
$r$: Yaw angle velocity
$r_b$, $r_c$, $r_s$: IP residuals
$s_r$: Sliding surface for yaw rate
$s_\beta$: Sliding surface for side-slip angle
$s_\sigma$: Sliding surface for SRC
$T_i$: Applied torque at the $i$th wheel
$\mathbf{u}$: Vector of allocated tire forces
$V$: Vehicle velocity
$v_{xi}$: Longitudinal velocity of the $i$th tire
$V_\beta, V_r, V_{\text{dyn}}, V_0$: Lyapunov candidate
$\mathbf{v}$: Vector of virtual control input
$\mathbf{W}$: Matrix of weighting coefficients
$X$: Body longitudinal force
$Y$: Body lateral force
$X_i$: Allocated longitudinal force to $i$th tire
$Y_i$: Allocated lateral force to $i$th tire
$Z_i$: Vertical load of $i$th tire.

*Greek Letters*

$\alpha_i$: Side-slip angle of $i$th tire
$\alpha_s^{\max}, \alpha_\lambda^{\max}$: Newton's step size
$\beta$: Side-slip angle
$\delta_i$: Steering angle of $i$th tire
$\overline{\Delta}_\beta, \overline{\Delta}_r$: Uncertainty upper bound
$\eta_k$: Barrier parameter
$\Phi_\beta, \Phi_r, \phi_\sigma$: Boundary layer thickness
$\boldsymbol{\lambda}$: Vector of Lagrange multipliers
$\boldsymbol{\Lambda}$: Matrix of Lagrange multipliers
$\sigma$: Centering parameter
$\sigma_i$: Slip ratio of the $i$th tire
$\sigma^*$: Reference value of slip ratio
$\mu_i$ : Friction coefficient of $i$th tire
$\omega_r, \omega_\beta$: Disturbance terms
$\omega_i$: Angular velocity of $i$th tire.

*Subscripts/Superscripts*

aff: Affine scaling
$f$: Front
$r$: Rear
$d$: Desired value
+: N iteration
dyn: Dynamic.

*Coordinate System*

$(x, y, z)$: Moving coordinate attached to vehicle centre.

## References

[1] J. Wang and R. G. Longoria, "Coordinated and reconfigurable vehicle dynamics control," *IEEE Transactions on Control Systems Technology*, vol. 17, no. 3, pp. 723–732, 2009.
[2] H. Peng and J.-S. Hu, "Traction/braking force distribution for optimal longitudinal motion during curve following," *Vehicle System Dynamics*, vol. 26, no. 4, pp. 301–320, 1996.
[3] O. Mokhyamar and M. Abe, "Simultaneous optimal distribution of lateral tire forces for the model following control," *Journal of Dynamic system, Measurement, and Control*, vol. 126, pp. 753–763, 2004.
[4] M. Naraghi, A. Roshanbin, and A. Tavasoli, "Vehicle stability enhancement—an adaptive optimal approach to the distribution of tyre forces," *Proceedings of the Institution of Mechanical Engineers Part D: Journal of Automobile Engineering*, vol. 224, no. 4, pp. 443–453, 2010.
[5] J. H. Plumlee, D. M. Bevly, and A. Scottedward Hodel, "Control of a ground vehicle using quadratic programming based control allocation techniques," in *Proceedings of the American Control Conference (ACC '04)*, vol. 5, pp. 4704–4709, Boston, Mass, USA, 2004.
[6] P. Tøndel and T. A. Johansen, "Control allocation for yaw stabilization in automotive vehicles using multiparametric nonlinear programming," in *Proceedings of the American Control Conference*, vol. 1, pp. 453–458, Portland, Ore, USA, 2005.
[7] Y. Kou, *Developement and Evaluation of Integrated Chassis Control Systems*, University of Michigan, 2010.
[8] T. A. Johansen, "Optimizing nonlinear control allocation," in *Proceedings of the 43rd IEEE Conference on Decision and Control*, pp. 3435–3440, Atlantis, Paradise Island, Bahamas, 2004.

[9] J. Tjønnås and T. A. Johansen, "Adaptive control allocation," *Automatica*, vol. 44, no. 11, pp. 2754–2765, 2008.
[10] J. Tjoønnäs and T. A. Johansen, "Stabilization of automotive vehicles using active steering and adaptive brake control allocation," *IEEE Transactions on Control Systems Technology*, vol. 18, no. 3, pp. 545–558, 2010.
[11] J. Y. Wong, *Theory of Ground Vehicles*, John Wiley & Sons, New York, NY, USA, 2001.
[12] J. E. Slotine and L. Weiping, *Applied Nonlinear Control*, Prentice-Hall, Englewood Cliffs, NJ, USA, 1991.
[13] Y. Shibahata, "Progress and future direction of Chassis control technology," *Annual Reviews in Control*, vol. 29, no. 1, pp. 151–158, 2005.
[14] S. J. Wright, *Primal-Dual Interior-Point Methods*, SIAM, Philadelphia, Pa, USA, 1997.
[15] J. Nocedal and S. J. Wright, *Numerical Optimization*, Springer, New York, NY, USA, 2nd edition, 2006.
[16] S. Boyd and L. Vandenberghe, *Convex Optimization*, Cambridge University Press, Cambridge, UK, 7th edition, 2009.
[17] R. Rajamani, *Vehicle Dynamics and Control*, Springer Science, New York, NY, USA, 2006.
[18] M. Abe, *Vehicle Handling Dynamics: Theory and Application*, Elsevier, London, UK, 2009.